Geothermal potential of tunnel infrastructures – development of tools at the city-scale of Basel, Switzerland

Geothermal Potential of Tunnel Infrastructures – Development of Tools at the City-Scale for the city of Basel

Jannis Epting[1], Matteo Baralis[2], Rouven Künze[3], Matthias H. Mueller[4], Alessandra Insana[2], Marco Barla[2], Peter Huggenberger[1]

[1]Department of Environmental Sciences, Applied and Environmental Geology, University of Basel, Switzerland

[2]Department of Structural, Geotechnical and Building Engineering, Politecnico di Torino, Turin, Italy

[3]TK CONSULT AG, Zürich, Switzerland

[4]Kiefer & Studer AG, Reinach, Switzerland

Abstract

This work presents preliminary evaluation elements for geothermal potential assessment and thermal influences of planned tunnel infrastructures for the urban agglomeration of Basel (Switzerland). In dependence of the tunnel type (motorway or railway) as well as its location related to the geological and hydrogeological settings different solutions for Shallow Geothermal Energy systems (SGE) are investigated. 'Passive' and 'active' SGE have been evaluated, including heat-exchanging segments installed in tunnel lining structures and thermal exploitation of water circulating in culvert systems.

First results suggest that thermal activation of a planned railway tunnel is most efficient where it is located within groundwater-saturated zones of the unconsolidated rock deposits. In summer, thermal power of 3.7 and 1.4 MW can be exchanged from two 736 and 284 m-long tunnel sections, respectively. Accordingly, in standard heat pump operating conditions a thermal energy of 10.4 and 3.8 GWh can be delivered for 'cooling'. In winter, thermal power of 1.9 and 0.7 MW can be exchanged, respectively, and a thermal energy of 5.2 and 1.9 GWh can be delivered for 'heating'.

SGE within culverts reveals to be favorable in heating mode only and for sections where the motorway tunnel runs perpendicular to the regional groundwater flow field as well as high ambient groundwater temperatures. Under such conditions along a 320 m-long tunnel section thermal power of up to 0.4 MW can be provided in summer and 0.8 MW in winter, respectively, and a thermal energy of 1.1 GWh in summer and 2.1 GWh in winter, can be delivered.

Keywords

Geothermal potential; tunnel infrastructure; shallow geothermal energy systems (SGE); city-scale; city planning

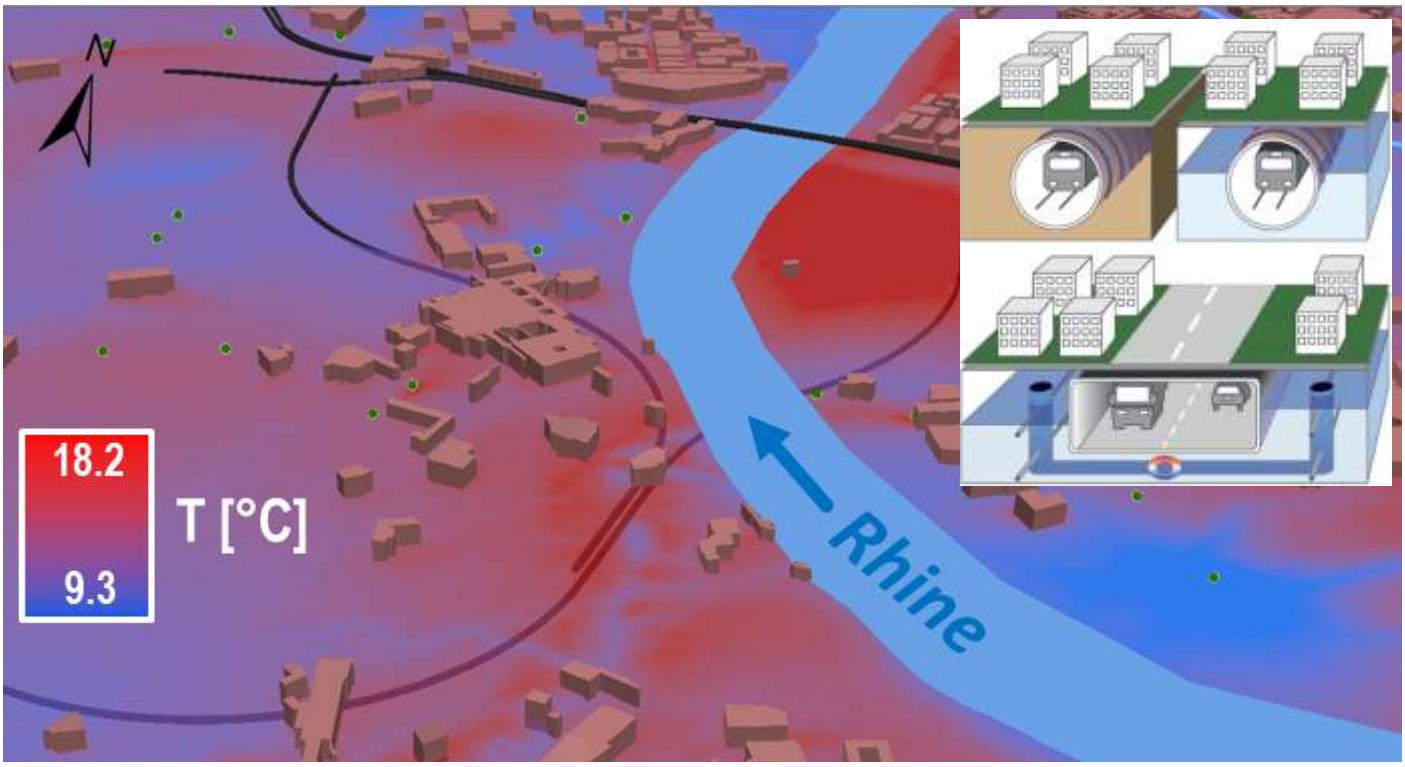

GA: Groundwater temperatures and urban subsurface constructions, including progression of planned and existent tunnels, at the bend of the river Rhine in the city of Basel, Switzerland. Upper right: Thermal exploitation of urban subsurface resources by means of 'passive' absorber SGE for railway tunnels (above) located within the solid bedrock (left) and partially groundwater-saturated unconsolidated rock deposits (right) as well as 'active' SGE within culverts for motorway tunnels (below) located within partially groundwater-saturated unconsolidated rock deposits.

Glossary

asl	above sea level
A_P	Pipe cross section Area [m^2]
BR	BedRock
bgs	below ground surface
C_f	volumetric thermal capacity fluid-phase (water) [MJ m^{-3} K^{-1}] as the product of specific heat capacity [4.20 x 10^6 kJ kg^{-1} K^{-1}] and the density of water at 10 °C [999,7 kg m^{-3}]
C_s	volumetric thermal capacity solid-phase [MJ m^{-3} K^{-1}]
SPF	Seasonal Performance Factor
d_{ext}	external diameter of pipe [m]
$P_{thickness}$	pipe wall thickness [m]
E_{adv}	advective energy transport by groundwater flow, corresponds to a heat flux per unit area, advective heat flux density [W m^{-2}]
E_n	Energy yield, normalized to activated tunnel surface [W m^{-2}]

GW	GroundWater
GWB	GroundWater Body
$\boldsymbol{k_f}$	hydraulic conductivity [m s^{-1}]
$\boldsymbol{k_{xx}}$	hydraulic conductivity x-direction
$\boldsymbol{k_{yy}}$	hydraulic conductivity y-direction
$\boldsymbol{k_{zz}}$	hydraulic conductivity z-direction
$\boldsymbol{n_{eff}}$	effective porosity
$\boldsymbol{q_i}$	flow through the circuit / conduit system [$kg\ s^{-1}$]
$\boldsymbol{Q_i}$	exchanged thermal power [kW]
$\boldsymbol{\Delta T}$	Temperature spread [K]
SGE	Shallow Geothermal Energy
$\boldsymbol{S_s}$	specific storage [m^{-1}]
SUHI	Subsurface Urban Heat Island
TAS	Tunnel Absorber Segment
TBM	Tunnel Boring Machine
$\boldsymbol{T_{in}}$	circuit inlet Temperature [°C]
$\boldsymbol{T_{out}}$	simulated circuit outlet Temperature [°C]
$\boldsymbol{TR_{\mathbf{heat,In}}}$	Transfer Rate heat In [W m^{-2} K^{-1}]
$\boldsymbol{TR_{\mathbf{heat,Out}}}$	Transfer Rate heat Out [W m^{-2} K^{-1}]
$\boldsymbol{TR_{\mathbf{,fluid,In}}}$	Transfer Rate fluid In [s^{-1}]
$\boldsymbol{TR_{\mathbf{fluid,Out}}}$	Transfer Rate fluid Out [s^{-1}]
TS	Tunnel Section
$\boldsymbol{v_h}$	heat carrier fluid velocity [m s^{-1}]
3D-TH model	3D Thermal Hydraulic Model
$\boldsymbol{\alpha_L}$	longitudinal aquifer thermal dispersivity [m]
$\boldsymbol{\alpha_T}$	transverse aquifer thermal dispersivity [m]
$\boldsymbol{\lambda_f}$	thermal conductivity fluid-phase [W m^{-1} K^{-1}]
$\boldsymbol{\lambda_s}$	thermal conductivity solid-phase [W m^{-1} K^{-1}]

Introduction

The socioeconomic development of metropolitan areas is accompanied by increasing traffic volumes also due to the high number of daily commuters from suburban areas and the countryside. As open space in urban areas is becoming scarce new infrastructure are increasingly being planned and constructed in the subsurface in response to high request of mobility. Likewise, many densely urbanized areas worldwide experience the Subsurface Urban Heat Island (SUHI) effect due to the more frequent thermal use of subsurface

resources for cooling purposes and heat introduced by asphalt ground surfaces and subsurface structures (buildings, motorway or railway tunnels, etc.; e.g. in Winnipeg, Canada (Ferguson and Woodbury, 2007); Cologne; Berlin, Munich, Cologne, Frankfurt, Karlsruhe and Darmstadt, Germany (Benz et al., 2015; Menberg et al., 2013; Zhu et al., 2011), respectively). Likewise, noticeably elevated groundwater temperatures of up to 16 to 18 °C were observed also in Basel (Epting and Huggenberger, 2013). For that reason, new subsurface use and infrastructure development should not lead to further thermal pollution of groundwater resources. However, the current often unregulated approach to energy resources management contradicts a sustainable development, especially in urban areas. Epting et al. (2018b) demonstrated that from a theoretical point of view aquifers could be directly exploited to exchange heat and store thermal 'waste energy'. This 'waste energy' of shallow urban subsurface has been related to an extremely high theoretical potential and preliminary technical solutions for its exploitation have been evaluated (Epting et al. submitted 2019).

Underground geotechnical structures, such as deep and shallow foundations, diaphragm walls, tunnel lining and anchors are being increasingly employed as energy geostructures worldwide (Laloui and Di Donna, 2013). Owing to the large ground-contacting surface of tunnel infrastructures, the thermal exploitation by means of a multitude of SGE is appealing. However, little attention has been paid to thermoactive urban tunnel infrastructures (Barla and Perino, 2014). Major reasons for this situation is that thermal activation is practicable only for new tunnels, and in addition to this such traffic infrastructure planning needs to be linked to urban energy management strategies. Further reasons involve high uncertainties related to site-specific conditions which strongly affect the efficiency of such systems (Bidarmaghz et al., 2017; Di Donna and Barla, 2016).

In Epting et al. (2018a) and Epting et al. (2018b) the advective heat transport with groundwater flow in highly permeable unconsolidated rock deposits was found to be the most important heat transport process in the redistribution of energy in the subsurface. Furthermore, urban settings often involve extremely transient groundwater flow and thermal regimes and multiple interactions may take place with other existing thermal or non-thermal users of the aquifer or with large underground structures. Therefore, these aspects have to be considered when dealing with linear underground infrastructures.

Among passive SGE, heat-exchange Tunnel Absorber Segments (TAS) can be used instead of traditional segmental lining (Lee et al., 2012; Moormann et al., 2016; Nicholson et al., 2014). The thermal activation is achieved by embedding a network of absorber pipes in the structural element. Hence a fluid circulating within the pipes extracts or injects heat from or into the ground. Recent studies have considered the application of this technology to tunnel linings, investigating feasibility and efficiency issues (Barla and Di Donna, 2018; Barla et al., 2018; Barla et al., 2019; Barla et al., 2016; Barla and Perino, 2014; Di Donna and Barla,

2016; Franzius and Pralle, 2011; Lee and Lam, 2012; Mimouni et al., 2013; Nicholson et al., 2013; Tinti et al., 2017; Zhang et al., 2013). Very few cases of real implementation or site-scale experiments of energy tunnels are known (Adam and Markiewicz, 2009; Barla et al., 2017; Franzius and Pralle, 2011; Frodl et al., 2010; Schneider and Moormann, 2010). Currently about 10 tunnel geothermal plants are operative (Buhmann et al., under revision), some of them are operated as pilot plants (Barla and Insana, 2018; Buhmann et al., 2016) and only a few are connected to real thermal users (Buch and Erichsen, 2017; Islam et al., 2006; Nicholson et al., 2014).

Despite the higher safety concerning environmental impact, passive SGE have usually lower efficiency compared to active open SGE. Among active SGE, thermal exploitation of water circulating in culvert systems can be pursued. Culvert systems are often necessary as technical measures to enhance groundwater exchange beyond the construction, avoid backwater effects and the development of stagnating groundwater zones along tunnel infrastructure (Epting et al., 2008b).

This work focuses on the application of such passive and active SGE to urban railway and motorway tunnels planned in the city of Basel, Switzerland. Based on local- and city-scale high-resolution 3D groundwater flow and heat-transport modeling (3D-TH model), the evaluation of tunnel thermal potential is presented. In both, the local- and the city-scale 3D-TH models, the site-specific hydrogeological conditions as well as the transient hydraulic and thermal boundary conditions are considered. For the quantification of exchangeable heat of different urban railway and motorway tunnels, representative cross-sections are studied by mean of local-scale 3D-TH models. The results of the local-scale 3D-TH models are subsequently upscaled to the city-scale to evaluate the regional impact of the tunnel infrastructures as well as the interaction with other subsurface and groundwater uses.

The advanced performance analysis of tunnel infrastructure represents the first step for spatiotemporal optimization in their thermal use under realistic settings.

Planned urban tunnels in the city of Basel

The city of Basel, Switzerland, at the border between France and Germany is experiencing high traffic volumes due to fast socioeconomic development and a high number of daily commuters. Similarly to most urban areas, open space is scarce and new infrastructures are increasingly being planned and constructed underground. Figure 1 shows the planned tunnel infrastructures in the urban region of Basel, Switzerland, for which the geothermal potential were assessed. Also illustrated is the progression of the tunnel through

the unconsolidated rock deposits and the bedrock as well as locations of planned subway stations and tunnel portals.

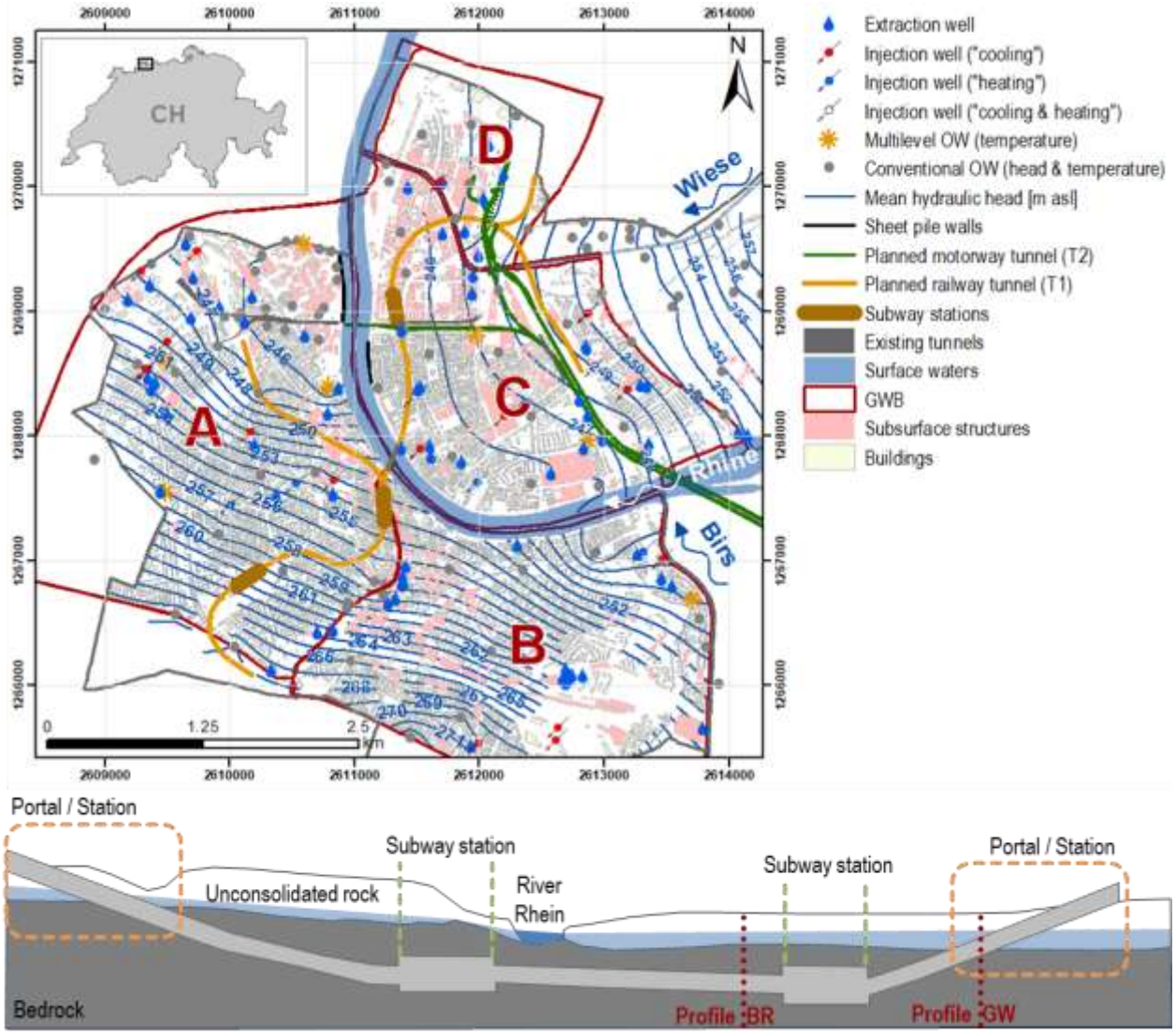

Fig. 1: Above: Urban GWB sub-units (A – D) and location of planned tunnel infrastructures in the city of Basel, Switzerland. Mean interpolated groundwater isolines for the years 2010 to 2015 (modified after Mueller et al. (2018)). Below: Sketch of the cross section of the lower and right part of the planned railway tunnel (T1).

In the city of Basel two main projects are at the feasibility study stage at the time of this work. The first one is a 5960 m long twin railway tunnel (T1) to connect three remote railway stations which are located on both sides of the Rhine. Along the railway tunnel T1 also three subway stations are planned (Fig. 1). The second one is a 6445 m long road tunnel (T2) which is being planned to increase the capacity of the motorway system to France and Germany. The portal sections of the tunnels are planned to be realized with the cut-and-cover

method and with injection tube screens within the unconsolidated rock deposits. At the interface to the bedrock and within the bedrock itself the tunnels will be excavated by a Tunnel Boring Machine (TBM).

Table 1 summarizes this partition into tunnel sections, which are in the groundwater-saturated zone of the unconsolidated rock deposits or in the bedrock.

Table 1: Dimensions of planned twin rail- (T1) and motorway (T2) tunnels located within the different GWBs and potential 'passive' TAS (inner and outer lining) and 'active' SGE and culverts (cf. Figs. 1 and 2).

GWB	Tunnel	SGE	Tunnel section	length [m]	Contact area [m²]
A	**T1**	'passive'	GW*	736	24'378
			BR**	2'728	89'768
C & D	**T1**	'passive'	GW*	284	8'922
			BR**	2'215	69'586
	T2	'active'	GW* (TS^{++} 2)	1'080	40'715
			GW* (TS^{++} 3)	425	16'022
			GW* (TS^{++} 4)	320	12'064
		-	BR	3'000	113'100
SE^{+}	**T2**	'active'	GW* (TS^{++} 1)	1'000	37'700
		-	BR**	620	23'370

GW*: Groundwater; BR**: Bedrock; SE^{+}: SouthEast GWB (cf. Fig. 2); TS^{++}: Tunnel Section

Figure 2 shows the sections of the railway twin tunnel T1 and the motorway tunnel T2 which are located within the groundwater-saturated and non-saturated zone of the unconsolidated rock deposits or such which are located in the bedrock. Also shown are the locations for which local-scale 3D-TH models were setup along selected tunnel sections (GW & BR) as well as those tunnel sections (TS1-4) which were selected for studying SGE within culverts. The railway twin tunnel T1 runs largely within the bedrock at depth of up to 30 m below ground surface (bgs). It can be seen that parts of the northern ascending and descending sections are oriented perpendicular to the regional groundwater flow field. The motorway tunnel T2 is planned to run through the groundwater non-saturated and saturated unconsolidated rock deposits as well as within the bedrock. Whereas the two ascending and descending tunnel sections (TS 1 & 3) are located within the groundwater-saturated zone and are oriented parallel to the regional groundwater flow field, the other two tunnel sections TS 2 & 4 are partly positioned perpendicular to it.

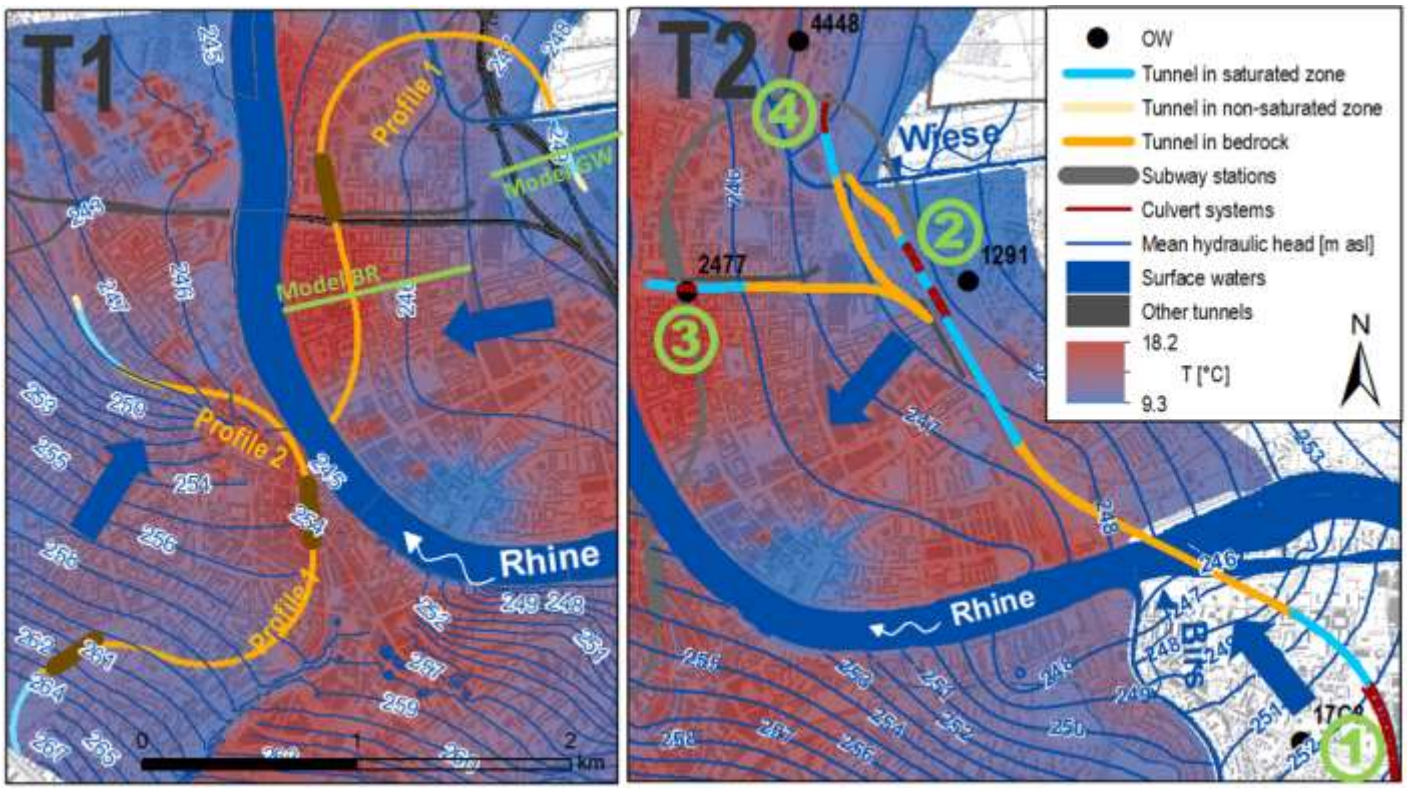

Fig. 2: Sections of the planned rail- and motorway tunnels. Mean simulated temperature and groundwater flow regime for the years 2010 to 2015 (modified after Mueller et al. (2018)). Blue arrows indicate the regional groundwater flow directions; for locations in the southeastern part no 3D-TH model exists, here groundwater heads are derived from an interpolation of measured data from groundwater observation wells (GeoView BL).

Conceptual approach & methods

Classification of tunnel infrastructures and thermal use concepts

The thermal design of energy tunnels requires the assessment of the amount of energy that a tunnel lining can exchange with the surrounding soil (Barla & Di Donna 2018, Baralis et al. 2018) by means of 3D-TH model where the thermal activation of the segmental lining can be simulated in detail.

Different conditions of tunnel infrastructures result in generally different internal air temperatures within railway and motorway tunnels. In fact, railway tunnels represent typical examples of ‘hot‘ tunnels due to ‘waste heat‘ introduced by train operation (braking, stopping at platforms and accelerating away from stations, e.g. Nicholson et al. (2014)). On the contrary, motorway tunnels can usually be classified as ‘cold’ tunnels due to low differences between internal air and ground temperatures.

Thermal influence on the surrounding ground is also directly linked to the presence of groundwater flow that affects the heat transport processes. Particularly in highly permeable unconsolidated sediments advective energy transport with groundwater flow (E_{adv}) is the most important heat transport process for the spatial redistribution of energy in the shallow subsurface. The quantification of this energy transport can be derived from city-scale 3D-TH models (Epting et al., 2018a; Epting et al., 2018b). Especially with the presence of groundwater flow, besides the use of 'passive' TAS, also 'active' use of E_{adv} is possible.

As regards the tunnels planned in Basel, the 'hot' railway tunnel T1 was studied with regards to 'passive' TAS. This solution was investigated for tunnel portals and intermediate subway stations (Figure 1 and 2). Furthermore, these sections present technical advantages as direct use of exchanged energy, sufficient room for heat pump installation and connection to the surface to possibly distribute excess heat exchange.

Regarding the planned large diameter motorway tunnel T2, investigations focused on tunnel parts which run within the partly groundwater-saturated unconsolidated rock deposits. At these locations culverts will be realized and their potential use by 'active' SGE is investigated.

Setup of city- and local-scale 3D-TH models

The setup as well as the calibration and validation of the numerical 3D-TH models are based on an extensive monitoring network present in Basel. The monitoring network involves, among others, more than 100 locations with continuous groundwater head and temperature measurements as well as 7 locations for high-resolution depth-oriented subsurface temperature measurements. Furthermore, modeling tools developed provide a deep understanding of thermal processes and transient of hydraulic and thermal boundary conditions which are relevant for the characterization of hydraulic and thermal regimes of the urban subsurface (Epting et al., 2018a; Epting et al., 2018b; Mueller et al., 2018). Based on the 3D-TH models the different natural and anthropogenic groundwater and heat exchanges could be quantified and the thermal potential derived for four delineated groundwater bodies (GWB) of Basel (Figs. 1 and 2). Thereby , a GWB is a distinct volume of groundwater that can effectively be managed and for which boundary conditions (hydraulic, thermal, chemical, etc.) can be delineated. Most urban aquifers comprise several isolated or connected GWBs. The knowledge of the thermal and hydraulic 'current state' of the investigated GWBs allows further evaluation of future changes, including the infrastructure projects presented in this study.

The original city-scale 3D-TH models were realized with unconsolidated rock and bedrock layers (FEFLOW©, Diersch (2014)). Adequate integration of the tunnel infrastructures with the geometry of the ascending and

descending parts within the mesh of the finite element numerical model was performed. Due to the complex geometrical features, locally an 'unstructured mesh' was adopted. This approach allows a spatially high-resolution in the vicinity of the tunnel infrastructures while optimizing computational efficiency by reducing the necessary number of mesh elements.

Particular attention was devoted to the up- and down-scaling procedure between local- and city-scale models. At first local-scale simulations were performed. Results included the transient temperatures at the extrados of the tunnel (Figure 3). Subsequently, these annual temperature time series were employed in the large-scale 3D-TH models as transient Dirichlet boundary conditions. Figure 2 shows the railway tunnel sections located within the groundwater saturated zone of the unconsolidated rock deposits and where the simulated temperature time series for the outer tunnel wall (extrados) of the local-scale 3D-TH model were employed (Figure 3, blue line). For those sections which are located within the bedrock, the simulated temperature time series for the outer tunnel wall (extrados) of the local-scale 3D-TH model were employed (Figure 3, dark red line). From the large-scale 3D-TH models the time series of the thermal budgets across the defined boundary conditions could directly be extracted for the different simulated tunnel sections and normalized to m^2 of tunnel surface as well as m tunnel length, accordingly.

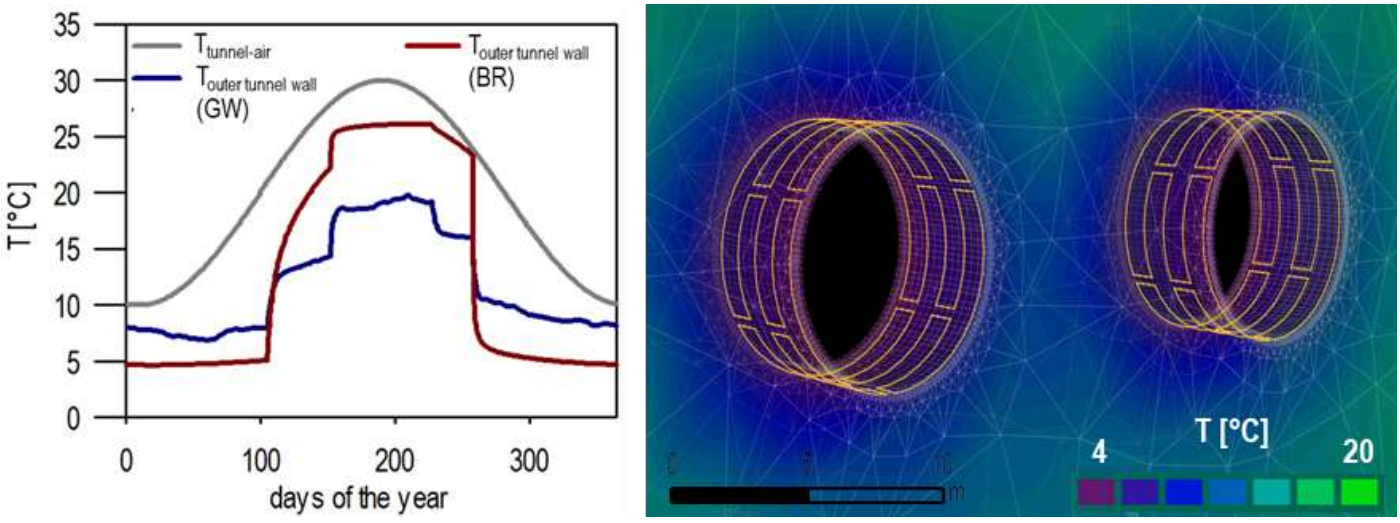

Fig. 3: Left: Analytically derived annual tunnel-air temperatures. Simulation results from the local-scale 3D-TH models and annual temperatures at the outer tunnel walls and the tunnel sections located in the groundwater (GW) and the bedrock (BR) which were employed as input functions (Cauchy-boundary conditions) for the individual tunnel sections of the city-scale 3D-TH models. Right: Zoom of the local 3D-TH model for the tunnel sections located in the bedrock during 'cooling' mode and discretization of the ENERTUN piping system in the lining segments (modified from Barla et al. (2016)).

On the basis of the city-scale 3D-TH models it was possible to identify locations that are relevant for further investigations by means of local-scale 3D-TH models. The tunnel tracks were analyzed and categorized depending on representative homogeneous conditions (Baralis et al., 2018). On the basis of these categories, corresponding local-scale numerical models were set up. As regards the planned twin railway tunnel T1 of 10 m diameter, two sections running completely within the bedrock or within the groundwater-saturated zone of the unconsolidated rock deposits, respectively, were selected (Fig. 2). These sections are also representative of conditions near planned subway stations (Fig. 1). The sections were chosen perpendicular to the regional groundwater flow field. In the vicinity of the chosen sections no groundwater user exist. Hence no affection on the hydraulic and thermal boundary conditions can be envisaged. In order to evaluate also the influence of the River Rhine (Fig 4), the local-scale 3D-TH model where the planned twin railway tunnel T1 is located in the bedrock was extended up to the river, resulting in a cross section length of 892 m. The 3D-TH model where the tunnel is located within the groundwater-saturated zone of the unconsolidated rock deposits has a length of only 540 m (Fig. 4). Both models are 1.4 m thick in order to include one ring of precast segments, as described below, and reach to 200 m asl (approx. 55 and 60 m bgs, respectively). Table S1 (supplementary information) summarizes the setup of the two local-scale 3D-TH models.

The up- and down-gradient model head and temperature boundaries were derived from groundwater monitoring wells, stage and temperature measurements within the river Rhine or from simulation results of the city-scale 3D-TH models. The upper (atmosphere) and lower (basal heat flux) boundary correspond to those of the city-scale 3D-TH models. Thermal interaction with internal air in the tunnels were modeled through Cauchy boundary conditions. In addition, the heterogeneous distribution of the aquifer properties is derived from the inversely calibrated and validated city-scale 3D-TH models (Table S1 within the supplementary information, Mueller et al. (2018)).

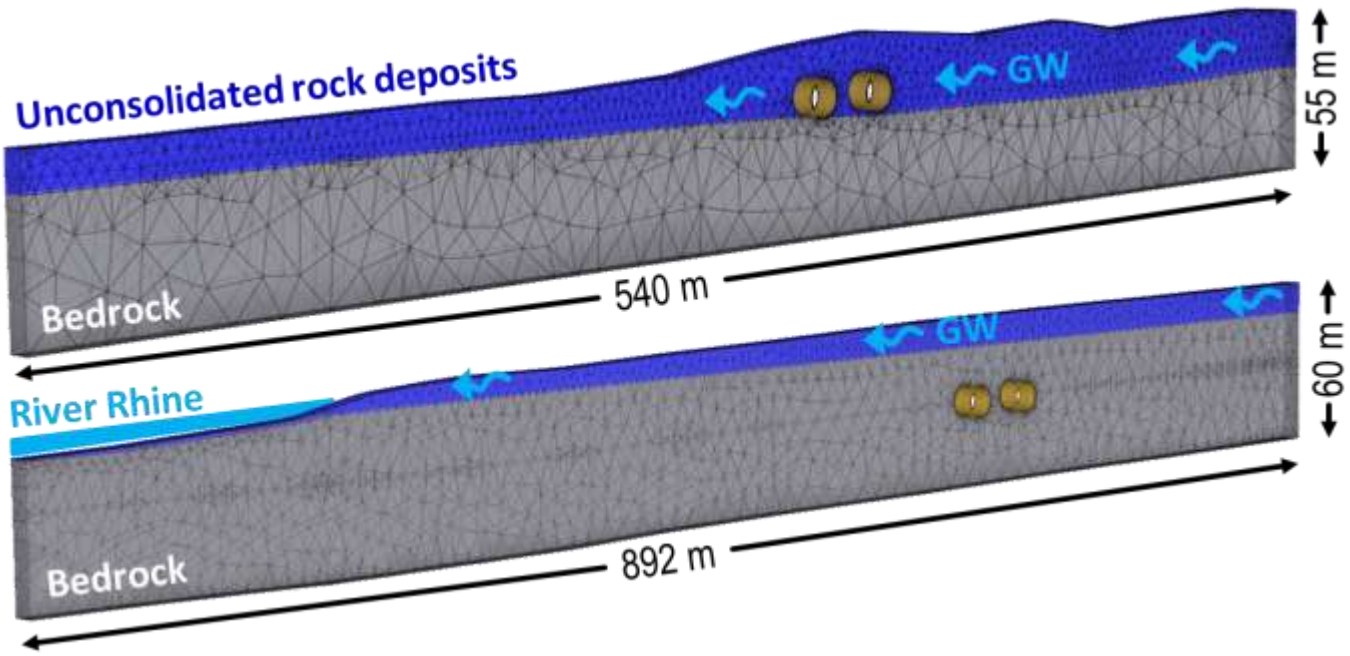

Fig. 4: Geometry of the two local-scale 3D-TH models where the investigated railway tunnel section is located completely within the groundwater (above) and the bedrock (below). Also shown is the regional groundwater flow direction within the non-consolidated rock deposits.

Energy tunnel segments

Today, a large number of urban tunnels are constructed by mechanized excavation where the tunnel lining is made up of precast segments installed by TBM. The segments can be prepared and optimized for heat exchange by including hydraulic circuits in the cast concrete (Barla et al., 2016; Frodl et al., 2010; Nicholson et al., 2014). As shown in Figure 3, the deployment of pipes network follows the scheme of the patented ENERTUN system (Barla and Di Donna, 2016). The ENERTUN system has already been technically and numerically validated in the different possible configurations for optimization of heat exchange with the ground or with the internal air (Barla et al., 2019; Barla et al., 2016; Di Donna and Barla, 2016). Both the “ground” and the “air” configurations can be also combined in a single segment. The first one is conceived for the thermal exchange with the ground while the latter configuration allows better efficiency in cooling the air inside the tunnel. The energy exchange of the system in the outer circuit takes place mainly with the ground (unconsolidated rock deposits or bedrock). Thus, the external system can be used to exploit the thermal potential of groundwater resources and as energy storage within bedrock layers. On the contrary, the energy exchange of the system in the inner circuit takes place mainly with the internal air. The internal tunnel air temperature was parameterized by a synthetic annual sinusoidal progression with temperatures reaching

10 °C in winter and 30 °C in summer (Fig. 3). Similar amplitudes for internal tunnel air temperature were observed in Torino Metro (Barla et al., 2016) and Paris Metro (RATP, 2010).

In order to simulate the embedded circuit of pipes in the FEFLOW© 3D-TH models, high-conductivity one-dimensional elements (named discrete features) were adopted. Geometry and properties of the pipes circuit were set according to the ENERTUN optimized scheme and derived from Barla and Di Donna (2016). Table S1 (supplementary information) summarizes the parameters adopted for the numerical models. Subsequently, thermal activation of the tunnel sections was investigated. The geothermal plant was assumed to operate continuously from 1 June to 15 August in cooling mode and from 15 September to 15 April in heating mode each year, in both tunnels simultaneously. In particular, the thermal activation was simulated imposing the heat carrier fluid to flow through the pipe circuits with a velocity of 0.7 ms^{-1} (flow through the circuit system approx. 0.2 ls^{-1}) during operation periods. The temperature of the heat carrier fluid entering the hydraulic circuit was set to constant values of 4 and 26.5 °C in the heating and cooling seasons, respectively (Baralis et al., 2018). The exchanged thermal power Q_i can be calculated according to:

$$Q_i[\mathrm{kW}] = C_f\ [\mathrm{kJ\ kg^{-1}\ K^{-1}}] * q_i\ [\mathrm{kg\ s^{-1}}] * \Delta T\ [K] \qquad \text{Eq. 1}$$

Where C_f is the specific heat capacity of water, q_i is the flow through the circuit system, ΔT is the temperature spread of the imposed circuit inlet T_{in} and the simulated outlet T_{out} temperature. In order to better compare the system efficiency, the energy yield E_n $[\mathrm{W\ m^{-2}}]$ can then be obtained by normalizing to the activated tunnel surface (Tab. 1).

Culvert systems

Tunnel constructions within the groundwater-saturated zone come along with backwater effects and the development of stagnating groundwater zones. Swiss regulations therefore demand technical measures to enhance groundwater exchange beyond the construction. These countermeasures include the installation of culverts or drawable sheet pile walls and slide pales (Epting et al., 2008a). Concerning the motorway tunnel T2 project, the latter option has been excluded because of the negative experience gained during the construction of a motorway tunnel infrastructure in Basel which was realized between 1994 and 2007. At that time 17 of the installed 100 slide pales (17 %) could not be drawn. Therefore, two-sided horizontal filters which are hydraulically connected to each other via a culvert conduit are envisaged.

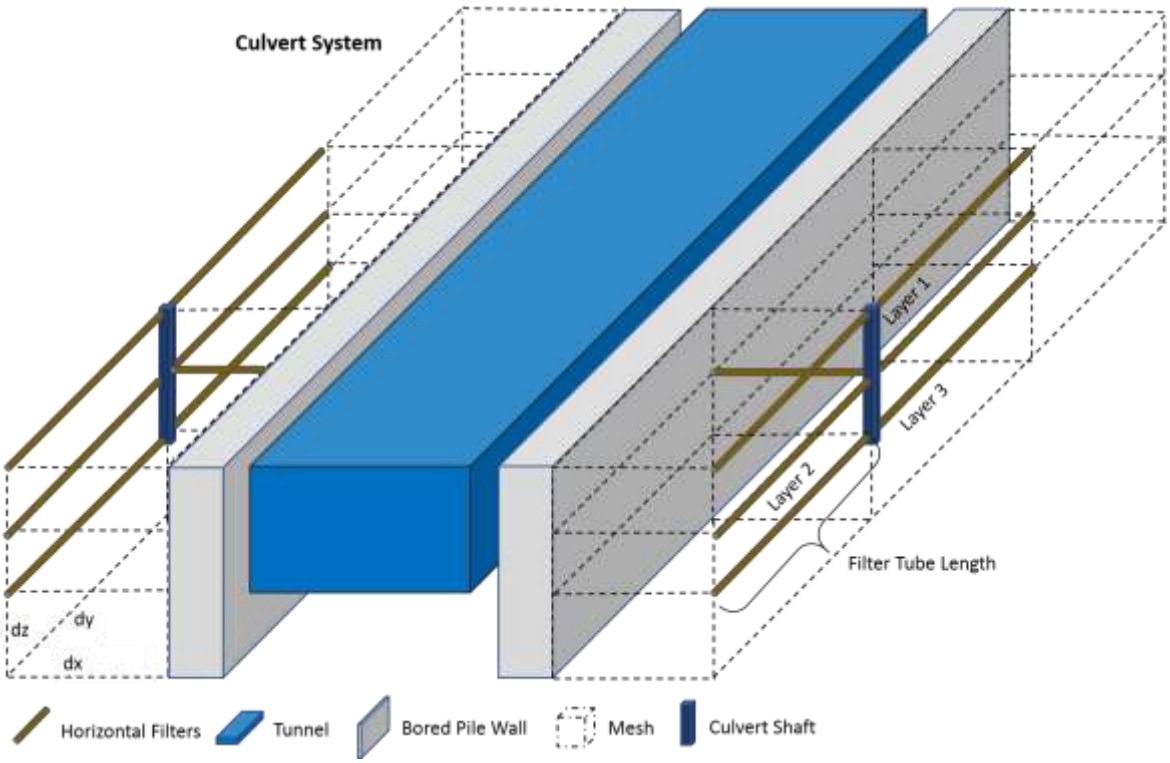

Fig. 5: Numerical model of the tunnel motorways and the culvert system.

Culverts must be designed in number and position that the natural flow regime can be approximately maintained. Hydraulic performance of different set-ups can be evaluated by a refined flow model with a thorough description of the tunnel and the building pit. Preliminar feasibility studies for the planned motorway tunnels (Tunnel Sections TS 1-4, Fig. 2 and Table 1) were performed by TK Consult based on a refined flow model of the unconsolidated rock using the groundwater model software SPRING (König et al., 2012). Figure 5 illustrates the numerical concept. The tunnel and the bored pile walls are represented by very low hydraulic permeability values. A continuous description of the tunnel geometry was realized by using an unstructured mesh with a vertical discretization length of 1 m. The culvert system is numerically described by zones of equal potential whereas the potential itself is obtained by solving the flow model. The method assumes negligible friction losses inside the culvert system while fully conserving mass. Simulations focused on the number of vertical filters and the distance between different culvert systems necessary to restore the natural flow regime. A maximum technically realizable filter tube length of 10 m was used. Two designs were for selected for evaluating resulting fluxes, the first refers to one-layered culvert systems with a distance of 10 m between the culverts, and a second (Figure 5) presents a three-layered system with an increased distance of 30 m. Both systems enable an almost complete reconstruction of the flow regime.

Results from these models were hence employed to evaluate the thermal potential from SGE installed within the culvert systems. Geothermal potential assessment has been performed including in equation 1 the simulated flow quantities (q_i) through the culvert systems. As regards the temperature spreads for summer and

winter, they were derived from groundwater temperature monitoring (Fig. 2) and assuming 'potential natural' groundwater temperatures equal to 10 °C. The thermal power Q_i has then been investigated for different hydrologic boundary conditions.

The first tunnel section (TS 1, Fig. 2) is located southeast of Basel; here the tunnel section is positioned mainly parallel to the regional groundwater flow field. Temperature measurements of a nearby groundwater observation well are relatively constant with a mean value of 12.2 °C and variations between 12 to 12.6 °C (time period 2006 to 2017; Observation Well (OW) 17C8, Fig. 2).

The second tunnel section (TS 2, Fig. 2) is located in GWB C; here the tunnel section is positioned perpendicular to the regional groundwater flow field. Temperature measurements of a nearby groundwater observation well show a relatively high variability between 8.8 to 15.1 °C and a mean value of 12.6 °C (time period 2006 to 2017; OW 1291, Fig. 2). Maximum values generally are measured in the winter and minimum values in the summer month, respectively.

The third tunnel section (TS 3, Fig. 2) is also located in GWB C near to the river Rhine; here the tunnel section is positioned parallel to the regional groundwater flow field. Temperature measurements of a nearby groundwater observation well are relatively constant with a high mean value of 16.8 °C and variations between 14.8 to 18.9 °C (time period 2010 to 2017; OW 2477, Fig. 2). Maximum values generally are measured in the early winter and minimum values in the summer month, respectively.

The fourth tunnel section (TS 4, Fig. 2) is located in GWB D; here the tunnel section is positioned oblique to the regional groundwater flow field. Temperature measurements of a nearby groundwater observation well show a relatively high variability between 12.6 to 17.8 °C and a mean value of 15.3 °C (time period 2006 to 2017; OW 4448, Fig. 2). Maximum values generally are measured in the early winter and minimum values in the early summer month, respectively.

Results

In the following the energy potential from energy tunnel segments on the city-scale derived from the high-resolution 3D-TH models and from the local-scale 3D-TH models as well as SGE in culvert systems is summarized.

City-scale energy potential from energy tunnel segments

Figure 6 shows heat exchanges standardized to 1 m^2 of tunnel surface area (Tab. 1) for the various tunnel sections of the planned railway tunnel located in the bedrock and within the groundwater-saturated zone in the different GWBs resulting from the city-scale 3D-TH models.

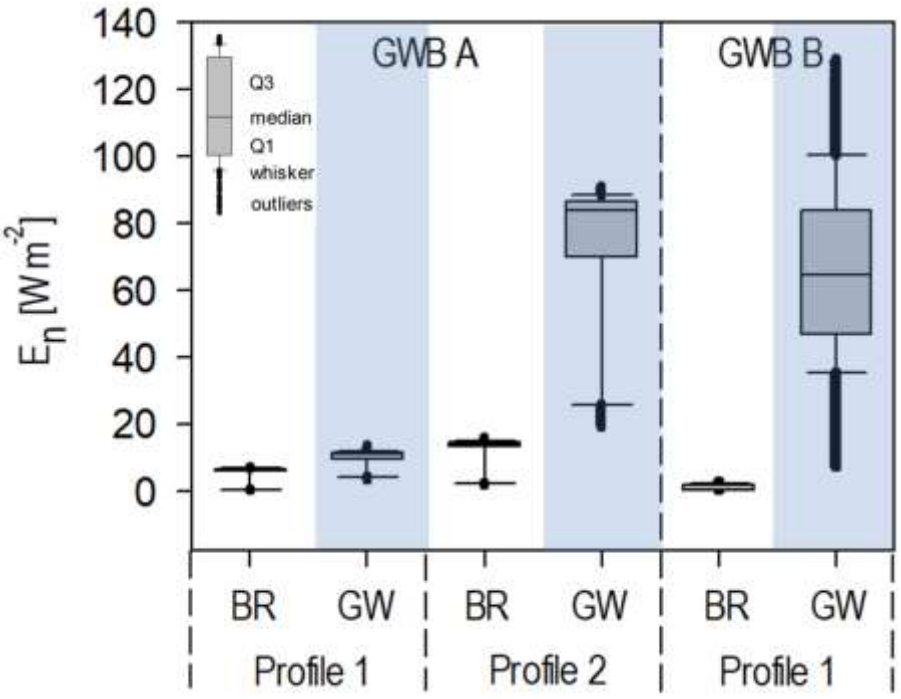

Fig. 6: Heat exchanges standardized to 1 m^2 of tunnel surface area for the various tunnel sections (TS) of the planned railway tunnel located in the bedrock (BR) and the groundwater-saturated zone (GW, blue shaded) along the profiles 1 and 2 (Fig. 2) in the different GWBs resulting from the city-scale 3D-TH models. The box plots show (see also imbedded sketch) the median (horizontal line within the gray shaded box), the quartiles Q1 and Q3 (shaded box), the upper and lower whiskers (horizontal bars outside of the box) as well as extreme outliers beyond the whiskers. Whiskers mark those values which are minimum and maximum unless these values exceed 1.5 times the inter quartile range (distance between Q1 and Q3).

For all tunnel sections which are located in the bedrock heat exchanges are comparatively small and below 15.6 W m^{-2}. As a result of a very thin groundwater layer for profile 1 in GWB A and for the tunnel section which is located within the groundwater-saturated zone running parallel to the regional groundwater flow field (Fig. 2), comparatively small heat exchanges below 9.7 W m^{-2} can be observed. On the contrary, for profile 2 in GWB A and for the tunnel section located within the groundwater-saturated zone running perpendicular to the regional groundwater flow field, relatively large mean heat exchanges of 71.6 W m^{-2} can be observed. The same can be observed for profile 1 in GWB B and for the tunnel section located within the groundwater-saturated zone. Also, this tunnel section runs perpendicular to the regional groundwater flow field, resulting in relatively large mean heat exchanges of 66.3 W m^{-2}. Moreover, as this tunnel section also

runs parallel to the river Wiese (cf. Fig. 2) the heat exchanges show a large annual variability (Fig. 7). Whereas part of this variability can be attributed to the operation regime, the thermal influence of the regional groundwater flow and thermal regime for the investigated time-period from 2010 to 2015 is evident. Beside a clear seasonality (with rising heat exchanges during the summer month and maximum values in autumn) also single characteristic flood events taking place in the individual years within the river Wiese can be observed. Likewise, during flood events in the nearby river Wiese in summer comparably 'warmer' and in winter comparably 'cooler' water infiltrates from the river into the aquifer, a process which has already been observed within wells for high-resolution multilevel temperature measurements along the river Rhine in GWB A (Epting and Huggenberger, 2013).

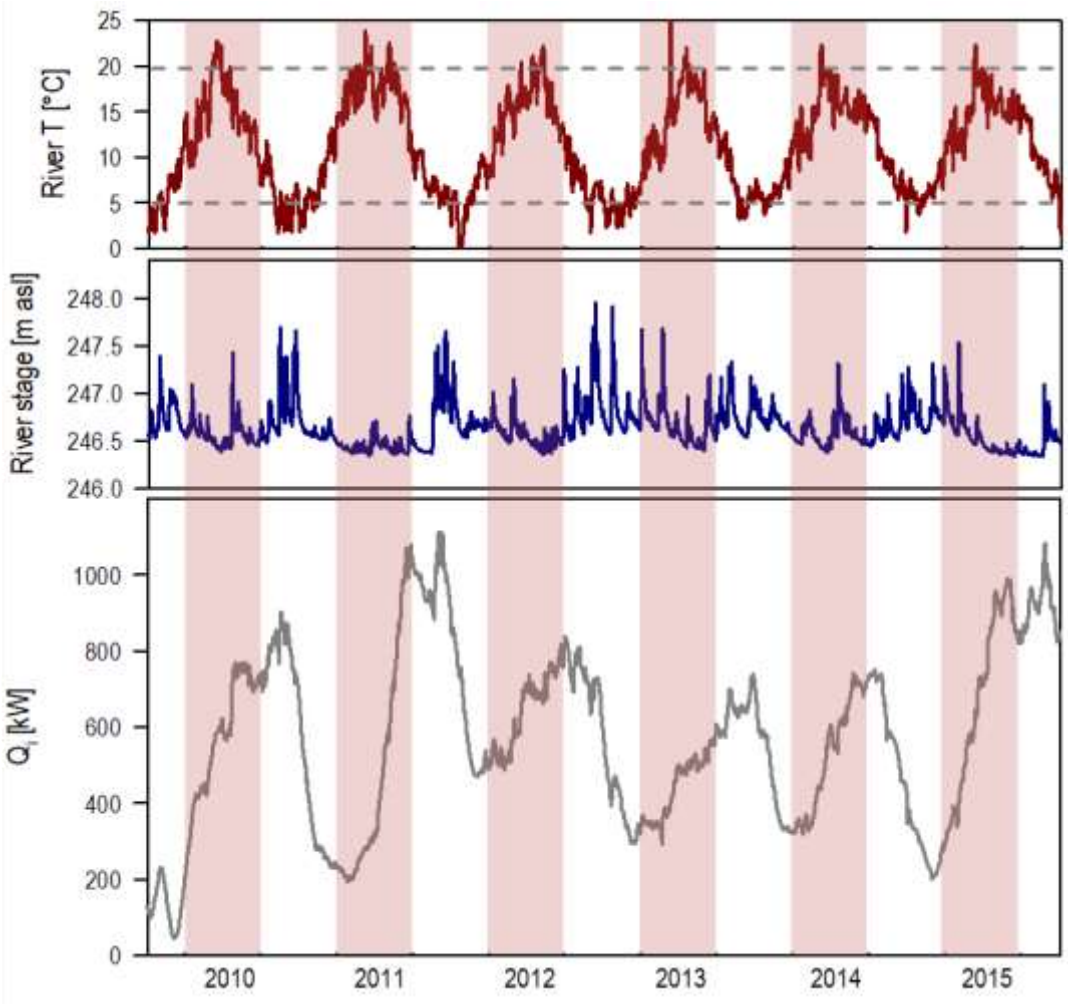

Fig. 7: Variability of total heat exchanges resulting from the city-scale 3D-TH model for profile 1 in GWB B and for the tunnel section located within the groundwater-saturated zone illustrated together with the temperatures (above) and stage (middle) of the nearby river Wiese.

Energy potential from energy tunnel segments

Figure 8 illustrates the inlet and outlet annual temperature profiles for the energy segments at the extrados of the tunnel lining. Highlighted are average temperature spreads representative for the different operation cycles. However, for more conservative estimates lowest temperature spreads should be applied. Temperature profiles for the interior installation are not presented additionally as they generally show the same progression as the ones for exterior installation with smaller temperature spreads (cf. Table 2). Figure 8 also shows selected simulated groundwater temperature time-series.

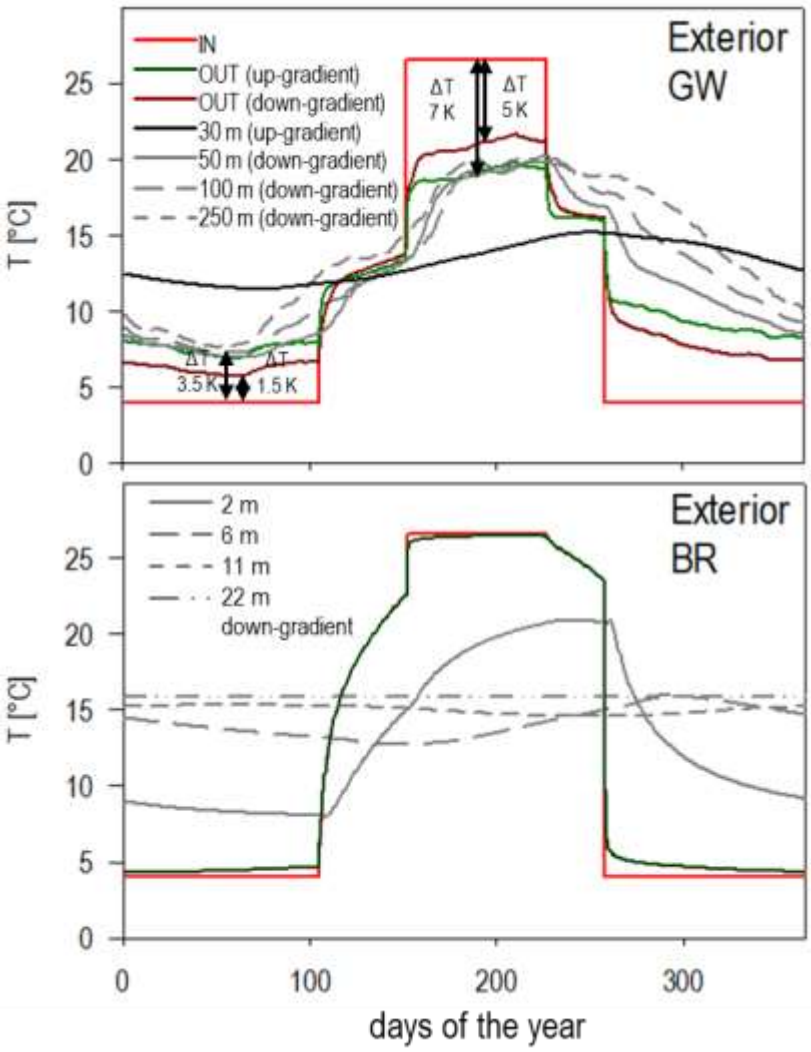

Fig. 8: Annual inlet (IN) and outlet (OUT) temperature profiles resulting from the local-scale 3D-TH models and the tunnel sections located in the groundwater (GW above) and the bedrock (BR below) for the exterior installation of ENERTUN within the tunnel lining. Also shown is the thermal impact at different distances down-gradient of the tunnel sections. For the tunnel section located within the GW results for the up- and downgradient tunnel sections as well as ambient GW temperatures up-gradient are presented.

As observed in Baralis et al. (2018) during operations, the outlet temperatures tend to reach asymptotically the inlet temperature. Although the trends were similar, a higher temperature difference occurs in cooling

mode. This is because the temperature difference with reference to the undisturbed condition is favorable for cooling. Furthermore, operating season in heating mode is longer, resulting in better performance for cooling mode operations. The square edged progression of the inlet and outlet temperatures can be attributed to the comparably fast groundwater flow velocities as also has been observed in the parametric study of (Bidarmaghz and Narsilio, 2018).

As the tunnel section which is located within the unconsolidated rock deposits runs parallel to the river Wiese, very high groundwater flow velocities can be observed. Likewise, mean Darcy flow amounts to 2 m d^{-1}; under consideration of a porosity of 0.12 this results in high fluid velocities of approx. 17 m d^{-1}.

Simulated groundwater temperature time-series 100 and 250 m down-gradient of the tunnel are above 19.7 °C (late summer) and below 7.3 °C (spring). Also shown is progression of ambient groundwater temperatures up-gradient of the tunnel which amount to a mean of 13.2 °C.

In Switzerland, the change of groundwater temperature 100 m down-gradient of a thermal impact is restricted to 3 K compared to a natural – anthropogenically unaffected – thermal state (GSchV, 2001). Therefore, the current operational setup of the thermal lining would have to be reconsidered in order to comply with the existing regulations.

Figure 9 shows the temperature distribution of the local-scale 3D-TH models for the thermally activated twin tunnels located completely within the groundwater-saturated zone and in the bedrock for summer and winter, respectively. For the thermally activated tunnel located in the groundwater-saturated zone the thermal plume associated to the ‘cooling’ (summer) and ‘heating’ (winter) mode is different.

Regarding the local-scale 3D-TH models for the thermally activated twin tunnels located completely within the bedrock a temperature corona around the tunnel can be observed which is more pronounced in summer during ‘cooling’ mode as a result of the larger temperature gradient of the activated tunnel in relation to the bedrock. However, the extension of the 15 °C isotherm is similar during summer and winter and comprise in a radius of 25 m from the twin tunnels (cf. Fig. 9). No thermal effects can be observed within the groundwater-saturated zone of the unconsolidated rock deposits.

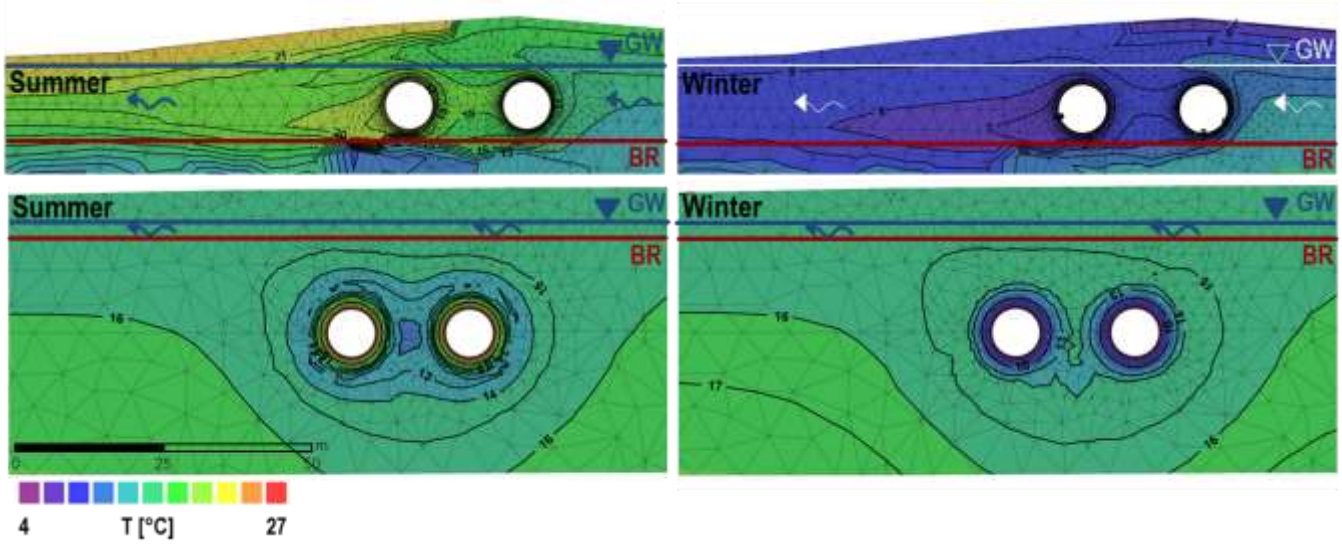

Fig. 9: Temperature distribution of the local-scale 3D-TH models for the thermally activated twin tunnels located completely within the groundwater-saturated zone (above) and in the bedrock (below) and for summer (left) and winter (right), respectively, for the second year of operation. Also shown is the progression of the bedrock and the simulated groundwater table.

Table 2 summarizes the results of the two local-scale 3D-TH models which simulated the thermal activation of the tunnel lining for the tunnel sections located within the groundwater-saturated zone of the unconsolidated rock deposits as well as within the bedrock layers. Both the interior and exterior configuration of ENERTUN and both the summer and winter seasons were considered. Energy yields $\mathrm{E_n}$ are normalized to 1 m^2 of tunnel surface. The resulting temperature spread ΔT for the up-gradient tunnel section located within the groundwater-saturated zone of the unconsolidated rock deposits and the exterior installation is about 7 K in summer and 3.5 K in winter mode, respectively. As a result of the observed very high groundwater flow velocities (see above) thermal power Q_i amounts to considerably high values of 6.7 and 3.4 kW and $\mathrm{E_n}$ of 152.9 and 76.5 W m^{-2}, respectively. Compared to the up-gradient installation, the resulting thermal potentials for the down-gradient installation are 71 and 43 % lower for summer and winter mode operation, respectively. The installation within the interior of the tunnel lining show a further reduction in efficiency of 43 to 67 % in dependence of up- and down-gradient installations as well as summer and winter mode operation, respectively.

Table 2: Simulated temperature spread as well as calculated thermal power and energy yield (normalized for tunnel surface and length) resulting from the local-scale 3D-TH models and the application of the ground and air circuits of the tunnel lining for summer and winter.

local-scale 3D-TH model	TAS ENERTUN lining	season	ΔT [K]	Q_i [kW]	E_n [W m^{-2}]	E_n [W m^{-1}]
TS in GW (up-gradient)	ground circuit	summer	-7	-6.7	-152.9	-4621.3
		winter	3.5	3.4	76.5	2310.6
	air circuit	summer	-4.0	-3.8	-87.4	-2640.7
		winter	1.5	1.4	32.8	990.3
TS in GW (down-gradient)	ground circuit	summer	-5.0	-4.8	-109.2	-3300.9
		winter	1.5	1.4	32.8	990.3
	air circuit	summer	-2.5	-2.4	-54.6	-1650.4
		winter	1.0	1.0	21.8	660.2
TS in BR (up- and down-gradient)	ground circuit	summer	0.0	0.0	0.0	0.0
		winter	0.5	0.5	10.9	330.1
	air circuit	summer	0.0	0.0	0.0	0.0
		winter	0.5	0.5	10.9	330.1

Baralis et al. (2018) observed that the efficiency in summer is higher due to the assumed higher difference between the inlet and soil temperatures with respect to the winter case. As a result of advective energy transport with groundwater flow (E_{adv}) the efficiency of the system is much higher, when located within the groundwater-saturated zone of the unconsolidated rock deposits.

Generally, the derived values are in the range of experience of other studies (Schlosser et al., 2007; Unterberger et al., 2004) even if different site conditions characterize this study. Indeed, depending on the respective geological, hydraulic and anthropogenic conditions, site-specific clarifications must be made. Brandl (2016) summarized energetic potential of different SGE, which is in the order of 10 to 30 W m^{-2} for flat absorber systems. For the currently operated 8 activated TAS worldwide heat flow rates between 6 and 170 W m^{-2} are documented (Moormann et al., 2018). Likewise, for the evaluation of the ENERTUN prototype performance in Turin (Italy) values of up to 51 W m^{-2} are documented (Barla et al., 2019).

Energy potential from culvert systems

Table 3 contains the resulting fluxes compiled for the two selected designs of one- and three-layered culvert systems. Both systems enable an almost complete reconstruction of the flow regime. Also summarized are

temperature spreads (ΔT) in winter and summer, respectively, which were derived from groundwater temperature monitoring under the assumption of 'potential natural' groundwater temperatures of 10 °C. The calculated thermal power Q_i refers to both average and elevated groundwater heads (cf. Eq. 1).

Table 3: Simulated flow through the culvert system as well as calculated temperature spread, thermal power and normalized energy yields resulting from SGE installed within culverts for summer and winter.

	season	q_i $[\mathrm{l\ s^{-1}}]$	ΔT [K]	$\mathrm{Q_i}$ MQ* [kW]	$\mathrm{Q_i}$ HQ** [kW]
TS 1 GWB SE⁺	summer	19 - 21	2	158 – 178	-
	winter		2.6	206 – 231	-
TS 2 GWB C	summer	11 - 14	-1.2	- 55 – -60⁺	- 65 – -69⁺
	winter		5.1	232 – 253	276 – 293
TS 3 GWB C	summer	< 1	2.8	8	7 – 8
	winter		7.8	24	22 – 25
TS 4 GWB D	summer	17 - 24	4.8	341 – 370	451 – 479
	winter		8.9	633 – 685	837 – 889

SE⁺: SouthEast GWB (cf. Fig. 2); MQ*: mean groundwater table; HQ**: high groundwater table; ⁺'cooling'

Despite considerably low ΔT in vicinity of tunnel section TS1 of only 2 K in summer and 2.6 K in winter and although the tunnel section largely runs parallel to the regional groundwater flow field, a relatively high thermal power Q_i for 'heating' of 168 kW in summer and 219 kW in winter, respectively, is achieved. Accordingly, section TS2, which runs perpendicular to the regional groundwater flow field with a comparably low ΔT of only 1.2 K in summer also leads to low Q_i of 55 to 69 kW during average and elevated groundwater head conditions. However, as ΔT is negative in summer groundwater resources could be used for 'free cooling'. On the contrary, a particularly high ΔT of 5.1 K in winter results in high Q_i of 243 kW during average and 285 kW during elevated groundwater head conditions. Regarding tunnel section TS3 which is positioned parallel to the regional groundwater flow field and despite a comparably high ΔT of 7.8 K in winter, calculated Q_i are generally low and range from 7 to 25 kW only during summer and winter and for the different investigated hydrological boundary conditions. High ΔT of 4.8 K in summer and 8.9 K in winter in vicinity of tunnel section TS4 which runs largely perpendicular to the regional groundwater flow field result in high calculated values of Q_i of 341 to 479 kW in summer and 633 to 889 kW in winter for the different investigated hydrological boundary conditions.

Table 4 summarizes first results as total energy yields E_n, seasonal heat exchanged and deliverable thermal energy by heat pumps for the exterior installation of ENERTUN and SGE installed within culverts. Energy yields for ENERTUN are extrapolated to the surface areas of the various railway tunnel sections located within the groundwater-saturated zone of the unconsolidated rock deposits and the bedrock (Tab. 1). Following the study of Miara et al. (2011), who performed a detailed analysis of Groundwater Heat Pump (GWHP) efficiency with different settings, we apply a conservative Seasonal Performance Factor (SPF) of 4 to calculate the deliverable thermal energy by heat pumps.

First results demonstrate that the thermal activation of the planned railway tunnels is most efficient where tunnel segments are located within the groundwater-saturated zone of the unconsolidated rock deposits. For two 736 and 284 m-long tunnel sections near the tunnel entrances, summer thermal power of up to 3.7 and 1.4 MW, respectively, could be generated. Hereafter, 7.8 and 2.9 GWh, respectively, thermal energy can be exchanged during the cooling season. Under the assumption of a SPF equal to 4, heat pumps could deliver 10.4 and 3.8 GWh, respectively, of thermal energy for cooling. Likewise, in winter thermal power of up to 1.9 and 0.7 MW, respectively, could be generated as well as 3.9 and 1.4 GWh, respectively, of thermal energy for 'heating'. Heat pumps could thus deliver, assuming a SPF of 4, 5.2 and 1.9 GWh of thermal energy for 'heating'. The length of tunnel sections which would have to be thermally activated within the bedrock to provide a substantial amount of energy illustrate the relative low efficiency of 'passive' SGE within the bedrock.

Table 4: Compilation of total energy yield, seasonal heat exchanged and deliverable thermal energy by heat pumps for the ENERTUN TAS (exterior of up-gradient tunnel section only) and SGE installed within culverts.

GWB	Tunnel Type	Tunnel section GW / BR	Energy yield		Seasonal heat exchanged [GWh]		Deliverable thermal energy by heat pump [GWh]	
			summer	winter	summer	winter	summer	winter
A	T1 railway twin tunnel	GW	3.7 MW	1.9 MW	7.8	3.9	10.4	5.2
		BR	0.0 MW	1.0 MW	0.0	2.0	0.0	2.7
C & D	T1 railway twin tunnel	GW	1.4 MW	0.7 MW	2.9	1.4	3.8	1.9
		BR	0.0 MW	0.8 MW	0.0	1.6	0.0	2.1
	T2 motorway tunnel	TS2 GW	62 kW	262.5 kW	0.1	0.5	0.2	0.7
		TS3 GW	7.5 kW	24.5 kW	0.0	0.1	0.0	0.1
		TS4 GW	410 kW	761 kW	0.9	1.6	1.1	2.1
SE**	T2 motorway tunnel	TS1 GW	168 kW	219 kW	0.4	0.5	0.5	0.6

** GWB SE: Groundwater body in the SouthEast (cf. Fig. 2); -COP = 4: Coefficient of Operation

Discussion

City and local-scale 3D-TH models are needed for the evaluation of different SGE application to tunnel infrastructures. The two types of models from this study show a valuable approach to determine the geothermal potential of the shallow urban subsurface. Indeed the local-scale 3D-TH models allowed investigation and evaluation of the operational and technical feasibility of TAS in different urban subsurface settings. The results show optimal use of the TAS setup in relation to the site-specific settings. The complementary application of the city-scale 3D-TH models allowed to derive the total geothermal potential when SGE systems are realized for the planned infrastructures. At scales the evaluation of the dynamics of hydraulic and thermal processes and the numerous interactions of the different natural and anthropogenic boundary conditions could be investigated and quantified. Since the city-scale 3D-TH models are calibrated and validated against high-resolution datasets covering main state variables for flow and heat transport problems, the uncertainty assumed is considerably lower than those using analytical approaches from other methods.

It has to be mentioned that the local-scale 3D-TH models were set up to reproduce settings of TAS for tunnel sections which run perpendicular to the regional groundwater flow field. Therefore, as tunnel sections within the regional 3D-TH models do not always run perpendicular to the regional groundwater flow field, energy yields will be to some extent lower as presented from the result of the extrapolation. Following the work by Buhmann et al. (under revision) for the TAS we could illustrate the relevance of the orientation of tunnel sections in relation to the regional groundwater flow field. Thereby, according to the VDI-Wärmeatlas (2006) for angles > 60 ° the effect of groundwater flow directions can be neglected. Concerning the efficiency of the TAS for single compared to twin tunnel systems the results of the up-gradient TAS would generally apply for single tunnel sections located within the groundwater-saturated zone of the unconsolidated rock deposits; for such tunnel sections located within the bedrock results for both TAS up- and down-gradient do not differ.

In comparison the installation of SGE within culverts for different sections of the planned motorway tunnels shows that only for locations where the tunnel runs perpendicular to the regional groundwater flow field and where the ambient groundwater temperatures are high a thermal exploitation (‘heating’ only) of groundwater resources is favorable. The best performance is obtained for tunnel section TS4 where, in dependence of the hydrological conditions, heat pumps could deliver thermal energy of 1.1 GWh in summer and 2.1 GWh in winter. A medium performance is obtained for a 1000 m-long tunnel section TS1 where, although the tunnel is positioned parallel of the regional groundwater flow field, heat pumps could deliver thermal energy of 0.5 GWh in summer and 0.6 GWh in winter, respectively.

Despite such encouraging energy potentials the equipment of tunnels with absorber technology often already fails in the design phase, since a forecast of the possible extraction rate under the very complex interactions of plant operation, geological and hydrogeological conditions as well as tunnel climate requires complex, mostly numerical simulations, which is not part of normal engineering practice (Moormann et al., 2018). Therefore, our results derived from city- and local-scale 3D-TH models illustrate how different natural and anthropogenic boundary conditions for the time-period of 2010 to 2015 allow not only evaluating the impact and thermal potential of tunnel infrastructures on the different spatiotemporal scales but also seasonality in relation to “heating” and “cooling” demand.

For example, the London clay and Paris alluvium and limestone ground, respectively, around metro tunnels have become unable to absorb the ‘waste heat’ from trains effectively. The consequence is that today’s temperature in many underground lines remains high throughout the year, with temperatures of more than 30 °C in some parts of the network (Botelle et al., 2010; RATP, 2010). Lining of ‘hot’ underground railway tunnels with TAS can provide a solution to cool the tunnels and surrounding ground, and transfer the harvested heat to adjacent buildings for heating (Nicholson et al., 2014). Therefore, different thermal use concepts (cooling, heating or both as well as thermal storage) can be envisaged for the different type of urban tunnel infrastructures. ‘Hot’ tunnels require cooling for which comparably colder surrounding ground within the deeper bedrock layers could be utilized. A further use of ‘heating’ energy from ‘hot’ tunnels can be the de-icing of infrastructures. On the contrary, for ‘cold’ tunnels energy concepts and low enthalpy geothermal plants for the thermal use of the observed SUHI within the unconsolidated rock deposits can be envisaged for ‘heating’ purposes.

Conclusions

The current development of energy geostructures lacks the scientific foundations and knowledge of how the various systems interact within the shallow subsurface and influence the hydraulic and thermal regimes in the subsurface. An essential difference to previous investigations on the thermal use of tunnel infrastructures is that in addition to the focus of energy production, other influencing factors such as regional hydraulic and thermal groundwater regimes and the diverse interaction in urban areas (groundwater uses, subsurface structures, etc.) were considered.

For tunnel sections, which are located in the groundwater-saturated zone of non-consolidated rocks and in the vicinity of tunnel portals, the installation of tunnel absorber systems (TAS) are particularly promising

because of comparatively high advective heat transport in these areas. Despite comparably lower efficiencies of SGE within culverts, culverts present an ideal infrastructure for SGE as they often have to be realized anyway. Also, the costs for new infrastructure or the construction of well doublets can be avoided. However, for culvert system technical maintenance opportunities have to be envisaged.

First results of this research project illustrate the applicability of the developed methods and tools to evaluate the general feasibility of the energetic use of tunnel structures. However, a realization for specific projects requires detailed studies to investigate their applicability.

Further work is required to include concepts of using thermal energy by tunnel infrastructure in the optimization of shallow energy resource management and an enhanced energy and spatial planning at the city level. Such management strategies should be based on sound scientific foundations for planning and decision-making.

Acknowledgements

We kindly acknowledge the financial support by the Swiss Federal Office of Energy for the research projects called 'Thermal Management Systems for the Shallow Subsurface of the Basel Region' and 'Feasibility Study: Thermal Potential of Urban Tunnelling Infrastructures in Unconsolidated Rock Groundwater Resources' (Swiss Federal Office for Energy SFOE-Project SI/501044-01 and SI/501646-01). Part of this work also was carried out in the framework of the European Cooperation in Science & Technology Action COST TU 1405, 'European network for shallow geothermal energy applications in buildings and infrastructures'. We also want to thank the Cantonal Agency of Environment and Energy Basel-City (AUE BS) for their cooperation in scope of diverse projects related to the thermal management of urban groundwater resources in the Basel area. Furthermore, gratefully acknowledge synergies work the Applied and Environmental Geology of the University of Basel performs in scope of the large-scale hydrogeological, geological and geotechnical investigations in relation to the planning of the tunnel infrastructure projects of the S-Bahn 'Herzstück' and the 'Rheintunntel' motorway.

References

Adam, D., Markiewicz, R., 2009. Energy from earth-coupled structures,foundations, tunnels and sewers. Géotechnique 59(3), 229-236.
Baralis, M., Barla, M., Bogusz, W., Di Donna, A., Ryżyński, G., Żeruń, M., 2018. Geothermal potential of the NE extension Warsaw (Poland) metro tunnels. Environmental Geotechnics, 1-13.
Barla, M., Di Donna, A., 2016. Concio energetico modulare prefabbricato, rivestimento per gallerie realizzato con una pluralità di tali conci e metodo per scambiare calore in una galleria mediante la realizzazione di un rivestimento con una pluralità di tali conci, Italian Patent (in Italian). Italian Patent 102 016 000 020 821, .
Barla, M., Di Donna, A., 2018. Energy tunnels: concept and design aspects. Underground Space 3(4), 268-276.
Barla, M., Di Donna, A., Baralis, M., 2018. City-scale analysis of subsoil thermal conditions due to geothermal exploitation. Environmental Geotechnics.
Barla, M., Di Donna, A., Insana, A., 2017. Energy tunnel experimental site in Turin Metro, Proceedings of the 15th IACMAG. Wuhan, China, pp. 1–10.
Barla, M., Di Donna, A., Insana, A., 2019. A novel real-scale experimental prototype of energy tunnel. Tunn Undergr Sp Tech 87, 1-14.
Barla, M., Di Donna, A., Perino, A., 2016. Application of energy tunnels to an urban environment. Geothermics 61, 104–113.
Barla, M., Insana, A., 2018. Energy Tunnel Segmental Lining: an Experimental Site in Turin Metro, in: Association, I.T.a.U.S. (Ed.) ITA - AITES WORLD TUNNEL CONGRESS.
Barla, M., Perino, A., 2014. Energy from geo-structures: a topic of growinginterest. Environ. Geotech 2(1), 3-7.
Benz, S.A., Bayer, P., Menberg, K., Jung, S., Blum, P., 2015. Spatial resolution of anthropogenic heat fluxes into urban aquifers. Science of the total Environment 524, 427-439.
Bidarmaghz, A., Narsilio, G.A., 2018. Heat exchange mechanisms in energy tunnel systems. Geomech Energy Envir 16, 83-95.
Bidarmaghz, A., Narsilio, G.A., Buhmann, P., Moormann, C., Westrich, B., 2017. Thermal interaction between tunnel ground heat exchangers and borehole heat exchangers. Geomech Energy Envir 10, 29-41.
Botelle, M., Payne, K., Redhead, B., 2010. Squeezing the heat out of London's Tube. P I Civil Eng-Civ En 163(3), 114-122.
Brandl, H., 2016. Geothermal Geotechnics for Urban Undergrounds. Procedia Engineer 165, 747-764.
Buch, C., Erichsen, C., 2017. Rosensteinstrassentunnel: Nutzung von Verlustwärme aus der Betriebszentrale in Verbindung mit Geothermie zur Klimatisierung von Gebäuden und Wasserbecken des zoologisch-botanischen Gartens Wilhelma, in: Richter, H., Theberath, J. (Eds.), U-Verkehr und unterirdisches Bauen, STUVA-Tagung 2017 - Internationales Forum für Tunnel und Infrastruktur. Forschung + Praxis, p. 433.
Buhmann, P., Moormann, C., Westrich, B., Pralle, N., Friedemann, W., 2016. Tunnel geothermics-A German experience with renewable energy concepts in tunnel projects. Geomech Energy Envir 8, 1-7.
Di Donna, A., Barla, M., 2016. The role of ground conditions on energy tunnels' heat exchange. Environ Geotech-J 3(4), 214-224.
Diersch, H.J., 2014. FEFLOW - Finite Element Modeling of Flow, Mass and Heat Transport in Porous and Fractured Media. Springer-Verlag Berlin Heidelberg.
Epting, J., Huggenberger, P., 2013. Unraveling the heat island effect observed in urban groundwater bodies - Definition of a potential natural state. Journal of Hydrology 501, 193-204.
Epting, J., Huggenberger, P., Rauber, M., 2008a. Integrated methods and scenario development for urban groundwater management and protection during tunnel road construction: a case study of urban hydrogeology in the city of Basel, Switzerland. Hydrogeology Journal 16(3), 575-591.
Epting, J., Mueller, M.H., García-Gil, A., Huggenberger, P., 2018a. Waste heat recovery – Considerations for the management of ther-mally polluted urban groundwater resources. Energy Geotechnics International Symposium on Energy Geotechnics SEG.
Epting, J., Mueller, M.H., Genske, D., Huggenberger, P., 2018b. Relating groundwater heat-potential to city-scale heat-demand: A theoretical consideration for urban groundwater resource management. Appl Energ 228, 1499–1505.
Epting, J., Regli, C., Huggenberger, P., 2008b. Groundwater protection in urban areas incorporating adaptive groundwater monitoring and management - Reconciliation of water engineering measures along rivers. Adaptive and Integrated Water Management: Coping with Complexity and Uncertainty, 97-123.
Ferguson, G., Woodbury, A.D., 2007. Urban heat island in the subsurface. Geophysical Research Letters 34(23).
Franzius, J.N., Pralle, N., 2011. Turning segmental tunnels into sources of renewable energy. P I Civil Eng-Civ En 164(1), 35-40.

Frodl, S., Franzius, J.N., Bartl, T., 2010. Design and construction of the tunnel geothermal system in Jenbach/Planung und Bau der Tunnel-Geothermieanlage in Jenbach. Geomech. Tunnell. 3(5), 658–668.
GSchV, 2001. Gewässerschutzverordnung (regulation for water protection). Switzerland.
Islam, M.S., Fukuhara, T., Watanabe, H., Nakamura, A., 2006. Horizontal U-Tube Road Heating System using Tunnel Ground Heat. Journal of Snow Engineering of Japan 22(3), 229-234.
König, C.M., Becker, M., Diehl, A., Rosen, B., Rüber, O., Seidel, T., Werth, B., Zimmermann, C., 2012. Benutzerhandbuch SPRING Version 4.1. Witten.
Laloui, L., Di Donna, A., 2013. Energy Geostructures: Innovation in Underground Engineering. ISTE Ltd and John Wiley & Sons Inc.
Lee, C., Park, S., Won, J., Jeoung, J., Sohn, B., Choi, H., 2012. Evaluation of thermal performance of energy textile installed in Tunnel. Renew Energ 42, 11-22.
Lee, C.K., Lam, H.N., 2012. A modified multi-ground-layer model for borehole ground heat exchangers with an inhomogeneous groundwater flow. Energy 47(1), 378-387.
Menberg, K., Bayer, P., Zosseder, K., Rumohr, S., Blum, P., 2013. Subsurface urban heat islands in German cities. Science of the total Environment 442, 123-133.
Miara, M., Günther, D., Kramer, T., Oltersdorf, T.-., Wapler, J., 2011. Heat pump efficiency: analysis and evaluation of heat pump efficiency in real-life conditions. Fraunhofer ISE.
Mimouni, T., Dupray, F., Minon, S., Laloui, L., 2013. Heat Exchanger Anchors for Thermo-active Tunnels, in: Experts, S.A.o.R.a.T. (Ed.). Zurich, Switzerland.
Moormann, C., Buhmann, P., Friedemann, W., Homuth, S., Pralle, N., 2016. Tunnel geothermics - International experience with renewable energy concepts in tunnelling / Tunnelgeothermie - Internationale Erfahrungen zu regenerativen Energiekonzepten im Tunnelbau. Geomechanics and Tunnelling 9(5), 467–480.
Moormann, C., Buhmann, P., Westrich, B., 2018. Web-based Application for the Investigation of thermally activated Tunnels. Tunnel Jg. 37.2018, Heft 6, 42-54.
Mueller, M.H., Huggenberger, P., Epting, J., 2018. Combining monitoring and modelling tools as a basis for city-scale concepts for a sustainable thermal management of urban groundwater resources. Science of the Total Environment 627, 1121–1136.
Nicholson, D.P., Chen, A.Q., Pillai, A., Chendorain, M., 2013. Developments in thermal pile and thermal tunnellinings for city scale GSHP systems, Thirty-Eight Workshop on Geothermal Reservoir Engineering. Standford University, Stanford, CA.
Nicholson, D.P., Chen, Q., de Silva, M., Winter, A., Winterling, R., 2014. The design of thermal tunnel energy segments for Crossrail, UK. P I Civil Eng-Eng Su 167(3), 118-134.
RATP, 2010. Appréciation de l'impact de la vitesse maximale des trains du Métro Grand Paris. Société du Grand Paris.
Schlosser, T., Schmidt, M., Schneider, M., Vermeer, P., 2007. Potenzial der Tunnelbaustrecke des Bahnprojektes Stuttgart 21 zur Wärme- und Kältenutzung, Schlussbericht. Universität Stuttgart.
Schneider, M., Moormann, C., 2010. GeoTU6-a geothermal Research Project forTunnels. pp. 14-21.
Tinti, F., Boldini, D., Ferrari, M., Lanconelli, M., Kasmaee, S., Bruno, R., Egger, H., Voza, A., Zurlo, R., 2017. Exploitation of geothermal energy using tunnel lining technology in a mountain environment. A feasibility study for the Brenner Base tunnel - BBT. Tunn Undergr Sp Tech 70, 182-203.
Unterberger, W., Hofinger, H., Grünstäudl, T., Adam, D., Markiewicz, R., 2004. Utilization of Tunnels as Source of Ground Heat and Colling – Practical Applications in Austria. Proceedings of the ISRM International Symposium 3rd ARMS, Kyoto, 421–426.
VDI-Wärmeatlas, 2006. 10th Edition, VDI Buch. Springer, Berlin.
Zhang, G., Xia, C., Sun, M., Zou, Y., Xiao, S., 2013. A new model and analyticalsolution for the heat conduction of tunnel lining ground heat exchangers. ColdReg. Sci. Technol 88, 59-66.
Zhu, K., Blum, P., Ferguson, G., Balke, K.D., Bayer, P., 2011. The geothermal potential of urban heat islands (vol 5, 044002, 2010). Environ Res Lett 6(1).

Table S1: Setup of the local-scale 3D-TH models, including hydraulic and thermal boundary conditions as well as the parameterization of the tunnel lining and ENERTUN (Baralis et al., 2018).

Parameter	Numerical realization
Hydraulic and thermal aquifer properties Value ranges derived from city-scale 3D-TH models *calibrated values in italic*	**hydraulic conductivity k_f** bedrock (local-scale 3D-TH model GW & BR) k_{xx}= k_{yy}= k_{zz}= 1.2 * 10^{-14} m s^{-1} non-consolidated sediments (local-scale 3D-TH model-GW) *k_{xx}= 8.1 * 10^{-3} – 1.8 * 10^{-2} m s^{-1}; k_{yy}= 7.7 * 10^{-3} – 2.1 * 10^{-2} m s^{-1}; k_{zz}= 5.6 * 10^{-4} – 1.4 * 10^{-3} m s^{-1}* non-consolidated sediments (local-scale 3D-TH model-BR) *k_{xx}= 7.7 * 10^{-4} – 1.3 * 10^{-3} m s^{-1}* *k_{yy}= 2.6 * 10^{-3} – 3.8 * 10^{-3} m s^{-1}; k_{zz}= 8.6 * 10^{-5} – 2.1 * 10^{-4} m s^{-1}* effective porosity (GW) n_{eff}= 0.12 effective porosity (BR) n_{eff}= 0.05 specific storage S_s= 1 * 10^{-4} m^{-1} fluid-phase thermal conductivity λ_f* = 0.65 W m^{-1} K^{-1} solid-phase thermal conductivity (GW) λ_s* = 3 W m^{-1} K^{-1} solid-phase thermal conductivity(BR) λ_s* = 1.19 W m^{-1} K^{-1} fluid-phase volumetric thermal capacity* C_f= 4.2 MJ m^{-3} K^{-1} solid-phase volumetric thermal capacity* C_s= 2.52 MJ m^{-3} K^{-1} longitudinal aquifer thermal dispersivity α_L= 5 m transverse aquifer thermal dispersivity α_T= 0.5 m Transfer Rate heat In (local-scale 3D-TH model-GW) *$TR_{\text{heat,In}}$ = 1.4 – 16.9 W m^{-2} K^{-1}* Transfer Rate heat Out (local-scale 3D-TH model-GW) *$TR_{\text{heat,Out}}$ = 2.1 – 9.3 W m^{-2} K^{-1}* Transfer Rate fluid In (local-scale 3D-TH model- BR, only Rhine) *$TR_{\text{fluid,In}}$ = 2.1 * 10^{-4} – 1.7 * 10^{-3} s^{-1}* Transfer Rate fluid Out (local-scale 3D-TH model- BR, only Rhine) *$TR_{\text{fluid,Out}}$ = 7.4 * 10^{-4} – 3.0 * 10^{-3} s^{-1}* Transfer Rate heat In (local-scale 3D-TH model- BR) *$TR_{\text{heat,In}}$ = 7.9 * 10^{-2} m^{-2} K^{-1}* Transfer Rate heat Out (local-scale 3D-TH model- BR) *$TR_{\text{heat,Out}}$ = 8.7 * 10^{-2} m^{-2} K^{-1}*
Tunnel lining	hydraulic conductivity k_{xx}= k_{yy}= k_{zz}= 1 * 10^{-15} m s^{-1} specific storage S_s= 10^{-4} m^{-1} solid-phase thermal conductivity λ_s= 2.3 W m^{-1} K^{-1} solid-phase volumetric thermal capacity C_s= 2.19 MJ m^{-3} K^{-1}
ENERTUN	pipe cross section area A_p = 0.327 10^{-4} m^2 external diameter d_{ext}= 0.025 m pipe wall thickness $P_{thickness}$ = 0.0023 m heat carrier fluid velocity v_h= 0.7 m s^{-1} specific storage S_s= 10^{-4} m^{-1} fluid-phase thermal conductivity λ_f= 0.64 W m^{-1} K^{-1} fluid-phase volumetric thermal capacity C_f= 4.2 MJ m^{-3} K^{-1} longitudinal thermal dispersivity α_L= 5 m transverse aquifer thermal dispersivity α_T= 0.5 m
T_{air} [°C]	air temperature measured at the meteorological station Basel-Binningen (7°35'N, 47°32'W, MeteoSwiss 1940) realized as Cauchy upper boundary condition (calibrated transfer rates)
$T_{tunnel-air}$ [°C]	Internal tunnel air temperature parameterized by synthetic annual sinusoidal temperature progression (amplitude: 10 °C winter; 30 °C summer) Cauchy boundary condition with empirical value for the transfer rate of the air layer hydraulic conductivity k_{xx}= k_{yy}= k_{zz}= 1 * 10^{-3} m s^{-1} transfer rate heat In & Out $TR_{\text{heat,In}}$ = $TR_{\text{heat,Out}}$ = 30 W m^{-2} K^{-1}
Heat-Flux bedrock [J m^{-2} d^{-1}]	Calculated from temperature measurements at different depth during the realization of a deep drilling Heat-Flux boundary condition

*****The thermal parameters conductivity and capacity of the subsurface are considered isotropic following the Swiss Standard SIA 384/6